

## Supporting information

### **Dithiocarbazate–Zn(II) complexes for photodynamic therapy and chemotherapy against lung cancer**

*JunGang Deng<sup>a,1</sup>, YouRu Wu<sup>a,1</sup>, AiLi Li<sup>a,1</sup>, WeiPing Pan<sup>a</sup>, LiXia Hou<sup>a</sup>, DaQi Wu<sup>a</sup>, ZhenLei*

*Zhang<sup>b</sup>, Feng Yang<sup>b\*</sup>, Yi Gou<sup>a,c\*</sup>*

<sup>a</sup> The Laboratory of Respiratory Disease, Affiliated Hospital of Guilin Medical University, Guilin 541001, Guangxi, China.

<sup>b</sup> School of Chemistry and Pharmaceutical Sciences, State Key Laboratory for Chemistry and Molecular Engineering of Medicinal Resources, Guangxi Normal University, Guilin, 541004, P. R. China.

<sup>c</sup> Department of Respiratory Medicine, Affiliated Hospital of Guilin Medical University, Guilin 541001, Guangxi, China.

\* Corresponding Author

\* F.Y. E-mail: [fyang@mailbox.gxnu.edu.cn](mailto:fyang@mailbox.gxnu.edu.cn);

\* Y.G. E-mail: [sanchuanok@126.com](mailto:sanchuanok@126.com).

## Table of Contents

<b>Supplementary text: Experimental section</b> .....	S3
<b>Figure S1</b> .....	S10
<b>Figure S2</b> .....	S11
<b>Figure S3</b> .....	S12
<b>Figure S4</b> .....	S13
<b>Figure S5</b> .....	S14
<b>Figure S6</b> .....	S15
<b>Figure S7</b> .....	S16
<b>Figure S8</b> .....	S17
<b>Figure S9</b> .....	S18
<b>Figure S10</b> .....	S19
<b>Figure S11</b> .....	S20
<b>Table S1</b> .....	S21
<b>Table S2</b> .....	S22
<b>Table S3</b> .....	S24
<b>Table S4</b> .....	S25
<b>Table S5</b> .....	S28
<b>ESI References</b> .....	S32

## Experimental section

### Materials and instruments

ZnCl<sub>2</sub>, methyl hydrazinecarbodithioate, picolinaldehyde, 1-(pyridin-2-yl)ethanone, di(pyridin-2-yl)methanone, and quinoline-2-carbaldehyde were purchased from Sigma-Aldrich. Solutions for biological and all spectroscopic studies were prepared with solvents of HPLC grade. The cell lines including human lung carcinoma (A549 and Calu-1) and *cis*platin-resistant lung cancer cell line (A549/DDP) were purchased from Sigma-Aldrich. Antibodies for immunoblotting analysis (activated caspases-3, CDKN1A, and HIF1A) were purchased from Abcam Co. (China). FITC-Annexin V for apoptosis detection was purchased from Beyotime (Jiangsu, China). All other reagents were obtained from commercial sources and used as received without further purification.

Elemental analysis (C, H, and N) was performed using a LECO CHNS-932 analyzer. Fluorescence spectra and UV-vis absorption spectra were acquired using a Hitachi RF-4500 spectrofluorometer and a GENESYS 180 spectrophotometer, respectively. The X-ray crystallography data of the Zn(II) complexes was obtained on a Bruker SMART APEX2 system. The Zn(II) complexes were tested against lung cancer cells using the 96-array LEDs (blue,  $\lambda_{\text{irr}} = 470 \text{ nm}$ ,  $20 \text{ mW cm}^{-2}$ ). The cellular/3D tumor spheroids were observed using a Nikon (AX+N-STORM) confocal microscope. Proteomic analysis was performed on a nanoElute UHPLC (Bruker Daltonics, Germany) and a hybrid timsTOF Pro2 (Bruker Daltonics, Germany) with a CaptiveSpray nanoelectrospray ion source. Flow cytometric analysis was conducted on a Becton Dickinson FACScan flow cytometer. The relative purity of complexes **Zn1**–**Zn4** used in this work was >95%, as determined through elemental analysis and an HPLC instrument with a reversed-phase C18 column (Fig. S11).

### Synthesis and characterization of the Zn(II) complexes

Ligands HL1–HL4 were synthesized as reported.<sup>1-3</sup> The Zn(II) complexes were prepared by adding a methanol solution of ZnCl<sub>2</sub> (0.136 g, 1 mmol) to the methanol solution of the respective ligands (2 mmol) and stirring for 2 h at 65°C. The above

reaction solution was slowly evaporated at room temperature to obtain dark-brown blocky single crystals.

$[Zn^{II}(L1)_2]$  (**1**). Yield: 72%. *Anal.* Calcd for  $C_{16}H_{16}N_6S_4Zn$  (485.96): C, 39.54; H, 3.31; and N, 17.29. Found: C, 39.12; H, 3.53; and N, 17.02.

$[Zn^{II}(L2)_2]$  (**2**). Yield: 74%. *Anal.* Calcd for  $C_{18}H_{20}N_6S_4Zn$  (514.01): C, 42.05; H, 3.92; and N, 16.34. Found: C, 41.78; H, 4.05; and N, 16.11.

$[Zn^{II}(L3)_2]$  (**3**). Yield: 86%. *Anal.* Calcd for  $C_{26}H_{22}N_8S_4Zn$  (640.13): C, 48.78; H, 3.46; and N, 17.50. Found: C, 47.53; H, 3.57; and N, 17.36.

$[Zn^{II}(L4)_2]$  (**4**). Yield: 64%. *Anal.* Calcd for  $C_{24}H_{20}N_6S_4Zn$  (586.07): C, 49.18; H, 3.43; and N, 14.33. Found: C, 50.03; H, 3.55; and N, 14.12.

The crystallographic data for these Zn(II) complexes were obtained on a Bruker SMART Apex II CCD diffractometer with Mo-K $\alpha$  ( $\lambda = 0.71073$ ) radiation at 296 K. The experimental structures of these Zn(II) complexes were solved using direct methods, and all the nonhydrogen atoms were anisotropically refined using the *Olex-2* software.<sup>4</sup> All the H atoms were generated geometrically using the riding model. Cambridge Crystal Data Center (CCDC) deposition numbers: 2265560 for Zn2, 2265561 for Zn3, and 2265562 for Zn4.

## DFT calculations

The calculations of the studied complexes were determined in the Gaussian 16 suite.<sup>5</sup> The binding energy between the dimers formed by  $\pi \cdots \pi$  stacking interaction in these complexes is studied by energy decomposition analysis based on force field (EDA-FF) analysis. Geometry optimizations of the monomer structures in these dimers were realized by density functional theory (DFT) using TPSSh-D3(BJ) functional in conjunction with 6-311+G\*\* (for S, C, O, N, and H atoms) and Stuttgart-Dresden pseudopotentials SDD (for Zn(II) atom) basis sets in the gas phase. Time-dependent (TD) DFT method has been employed to investigate the electronic transition properties. Before performing the TD-DFT calculations, the ground state geometries of these complexes were optimized at the pbe1pbe/6-31G(d) level (6-31G(d) for S, C, O, N, and H atoms; SDD for Zn(II) atom) associated with the IEF-PCM model. The TD-DFT calculations were performed at the pbe1pbe basis set with IEF-PCM model. The 6-311G(d, p) basis on the nonmetal atoms coupled with SDD for zinc was employed in

the TD calculations. The EDA-FF analysis and the charge-transfer spectrum computations were performed using the Multiwfn software.<sup>6-8</sup>

### **Fluorescence imaging**

The cellular imaging of the Zn(II) complexes was conducted using a Nikon (AX+N-STORM) confocal microscope. In brief, A549 cells were seeded on glass bottom dishes and maintained in RPMI 1640 containing 10% fetal calf serum; 24 h after cell seeding, cells were incubated at 37 °C for 30–120 min with complexes Zn1–Zn4 (5 μM). Then, cells were washed three times with phosphate-buffered saline (PBS) to remove the excess of the Zn(II) complexes and kept in fresh RPMI 1640 for fluorescence imaging. The Zn(II) complexes were excited using the 488 nm laser, and their emission was detected from 520 to 570 nm.

### **Hemolysis assay**

Hemolysis assay was proceeded following a previously reported method.<sup>9</sup> Briefly, red blood cells were collected via centrifugation at 1500 rpm (10 min at 4°C) and then washed with PBS twice. The red-blood-cell pellet (1 mL) was resuspended in 3 mL of PBS. Then, 0.1 mL of diluted erythrocyte suspension was added to 0.5 mL of PBS solution containing various concentrations of each Zn(II) complex/*cisplatin*. All of the samples were incubated at 37°C. After 4 h, the samples were centrifuged at 12000 rpm (10 min at 4°C), and then, 100 μL of supernatant was taken from each sample to a 96-well plate to measure the absorbance at 570 nm. Control samples with 0% lysis (PBS) and 100% lysis (1% Triton X-100) were employed in this experiment. The percentage of hemolysis of red blood cells was determined as follows, hemolysis (%) =  $(A_s - A_n)/(A_p - A_n) \times 100\%$ , where  $A_s$ ,  $A_n$ , and  $A_p$  are the absorbances of the sample, negative control, and positive control, respectively.

### **Cell cytotoxicity assays**

The cells were cultured in McCoy's A5 (for human lung cancer cell line Calu-1) and RPMI 1640 (for human lung cancer cell lines A549 and A549cisR) cultures supplemented with 1% antibiotic–antimycotic solution and 10% fetal bovine serum in an atmosphere containing 5% CO<sub>2</sub> at 37°C.

Cytotoxicities in the dark and under light irradiation were determined for these Zn(II) complexes. White or black 96-well plates were seeded with about 5,000

cells/well and incubated for 24 h. For dark cytotoxicity, the cells were incubated with different concentrations (0–32  $\mu\text{M}$ ) of test complexes for 48 h. For photocytotoxicity, varying concentrations (0–10  $\mu\text{M}$ ) of the Zn(II) complexes were added to the cells, incubated for 2 h, washed with PBS, followed by 15 min of irradiation using blue LEDs (470 nm, 20 mW/cm<sup>2</sup>). After irradiation, the cells were incubated for a further 46 h in a complex-free medium. After that, a solution of MTT (10  $\mu\text{L}$ , 5 mg/mL) in PBS was added to each well of 96-well plates, and then, the plates were incubated for 4 h in 5% CO<sub>2</sub> at 37°C. Subsequently, the supernatant in each well of the 96-well plate was replaced with 100  $\mu\text{L}$  of dimethyl sulfoxide to dissolve the MTT–formazan crystals. The optical density of each well was measured at 570 nm using an Infinite M200 Pro microplate reader.

### **Detection of intracellular ROSs**

Intracellular ROS generation by the investigated Zn(II) complexes after irradiation was detected using a red fluorescence cellular ROS detection kit (abcam, ab186027). A549 cells were seeded on the 6-well plate and incubated overnight under 5% CO<sub>2</sub> at 37°C. The cells were incubated with the ROS probe ( $\lambda_{\text{ex}} = 520 \text{ nm}$ ,  $\lambda_{\text{em}} = 590\text{-}625 \text{ nm}$ ) for 1 h in the incubator and then treated with 5  $\mu\text{M}$  of the investigated Zn(II) complexes in the dark for 2 h. After 15 min of blue light irradiation (or incubation in the dark), the samples were washed with PBS and examined using fluorescence microscopy.

### **Analysis of 3D tumor spheroids**

Tumor spheroids were prepared with A549 cells by seeding 1,500 cells/well in Ultra-Low Attachment 96-well plates (Corning) in RPMI 1640. The culture medium was replaced every day. Within 2–4 days tumor spheroids were formed from the cell suspension. For imaging, tumor spheroids were incubated in normal medium with complex Zn3 (5  $\mu\text{M}$ ) for 24 h. Then, they were washed with PBS twice and observed using a Nikon (AX+N-STORM) confocal microscope. The fluorescence images along the z-axis were captured using ( $\lambda_{\text{ex}} = 488 \text{ nm}$ ,  $\lambda_{\text{em}} = 520 \text{ to } 570 \text{ nm}$ ) excitation in the Z-stack mode.

The inhibition of the growth of 3D tumor spheroids was assessed by measuring the size of tumor spheroids following treatment with different concentrations of complex Zn3. The 3D tumor spheroids were divided into two identical groups. The first

group was treated with different concentrations of complex Zn3 in the dark. The second group was used for photodynamic therapy analysis according to the previously reported method.<sup>10</sup> In brief, the second group was exposed to blue light irradiation (470 nm, 20 mW/cm<sup>2</sup>) for 15 min. After this exposure, tumor spheroids were suspended in fresh medium and imaged using microscopy (OLYMPUS Co., Japan). Second irradiation was performed as described above 24 h later. Finally, the spheroids were imaged after 72 h.

### **Selective scavenging of ROSs in A549 cells**

A549 cells were seeded on the six-well plates and incubated for 24 h. To determine the type of ROSs generated in A549 cells, the cells were pretreated with selective ROS scavengers, incubated for 1 h in 5% CO<sub>2</sub> at 37°C and subsequently treated with complex Zn3 (1.0 μM). Hydroxyl radicals (<sup>•</sup>OH) scavenged using 50 mM D-mannitol, hydrogen peroxide (H<sub>2</sub>O<sub>2</sub>) was scavenged using sodium pyruvate at the final concentration of 10 mM, singlet oxygen (<sup>1</sup>O<sub>2</sub>) was scavenged using 5 mM sodium azide, peroxyxynitrite anion (ONOO<sup>-</sup>) was scavenged using 50 μM ebselen, and superoxide anion radicals (<sup>•</sup>O<sub>2</sub><sup>-</sup>) were scavenged using 5 mM tiron.<sup>11</sup> The antioxidants remained throughout the experiment. After the pretreatment with selective ROS scavengers, the cells were treated for 2 h with complex Zn3. The cells were subsequently washed with PBS and exposed to blue light irradiation (470 nm, 20 mW/cm<sup>2</sup>) for 15 min. After irradiation, the cells were imaged using microscopy (OLYMPUS Co., Japan).

### **Proteomics analysis**

To establish a proteomics model for studying the chemotherapeutic mechanism of complex Zn3, A549 cells were treated with complex Zn3 (5 μM) or vehicle control for 24 h. After incubation, the cells were harvested and washed with cold PBS. The proteomics analysis was performed using the reported methods.<sup>12</sup> Briefly, first, protein extraction, digestion, and cleanup were performed. Subsequently, samples were fractionated using nanoliter flow rate nanoElute UHPLC system (Bruker Daltonics, Germany) and analyzed via timsTOF Pro2 LC-MS/MS. Finally, the database search, protein quantification, and bioinformatics analysis of these samples were performed. The MS raw data was processed using the DIA-NN(v1.8.1) software and the uniprot\_proteomeUP000005640\_human\_20230504.fasta database. Bioinformatics

analysis mainly focused on Gene Ontology annotation, subcellular localization, and KEGG pathways analysis.

### **Immunoblotting analysis**

A549 cells were seeded in 3.5 cm dishes and cultured for 24 h. After that, the cells were treated with the vehicle control or complex Zn3 (5 and 10  $\mu$ M). After 24 h, cells were harvested and lysed. The protein concentrations were determined using the BCA kit (Beyotime, Nanjing, China). Target proteins, including cleaved caspase-3 (Proteintech), PARP-1 (Abcam), cleaved PARP-1 (Abcam), ITGA5 (Abcam), MMP-9 (Abcam), CDKN1A (Abcam), HIF1A (Abcam), LTBR (Abcam), and GAPDH (Abcam), were incubated with the corresponding primary antibodies and subsequently imaged using a Cytiva ultrasensitive multifunction imager (Amersham ImageQuant 800).

### **Apoptosis**

Apoptosis of A549 cells was analyzed using the FITC-Annexin V kit (Beyotime, Jiangsu, China). A549 cells were seeded in six-well plates and cultured for 24 h. After that, the cells were treated with complex Zn3 (5 and 10  $\mu$ M) or the vehicle control for 24 h. The cells were then harvested, stained with Annexin V-FITC/PI, and observed via flow cytometry.

### **Cell cycle**

Cell cycle distribution was analyzed through propidium iodide (PI) staining and flow cytometry. The cells were treated with complex Zn3 (5 and 10  $\mu$ M) or the vehicle control for 24 h. After that, the cells were collected, washed twice with cold PBS, and fixed with 70% ethanol at  $-4^{\circ}$ C overnight. The cells were treated with RNaseA for 35 min at  $37^{\circ}$ C, followed by PI staining for 15 min in the dark. Cell cycle was analyzed through flow cytometry.

### **Scratch wound-healing assay**

A549 cells were seeded into six-well plates and cultured until approximately 90% confluence. Wound gaps in the monolayer cells were created using sterile pipette tips. Cell debris was carefully removed with cold PBS. Subsequently, cells were cultured for

24 h in RPMI-1640 medium containing 1% fetal bovine serum (to minimize cell proliferation during the assay) with or without complex Zn<sub>3</sub>.

### **Statistical analysis**

All experimental data are expressed as the mean  $\pm$  SD (standard deviation). The student's T-test and one-way analysis of variance (ANOVA) test were used for statistical analysis.

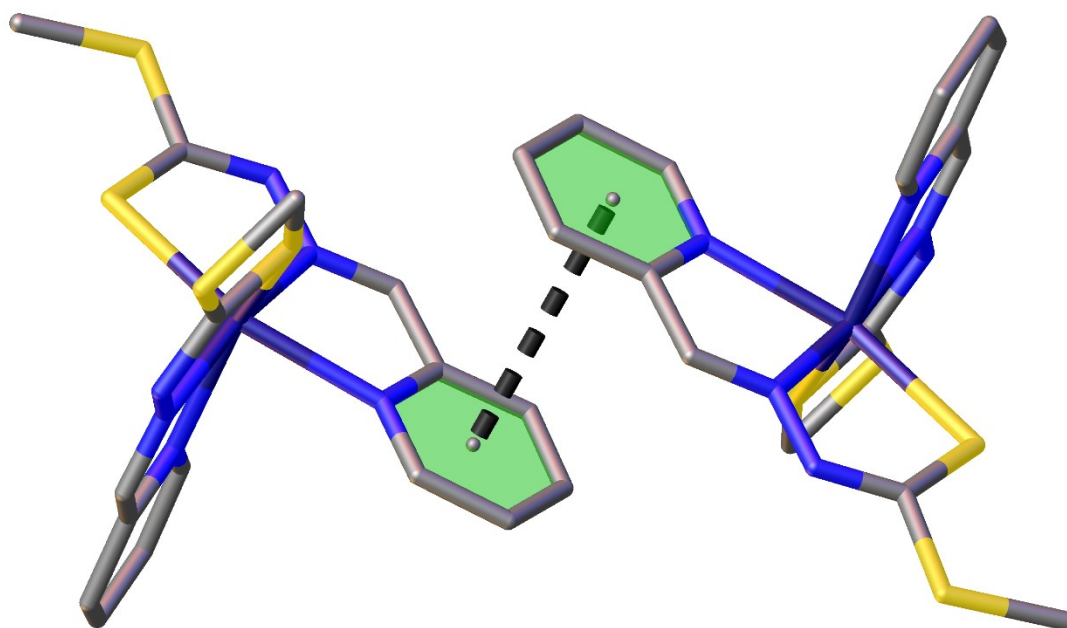


**Figure S1.** View of a dimeric structure formed by  $\pi \cdots \pi$  stacking interaction (dashed lines) in complex Zn1. The H atoms are omitted for clarity.

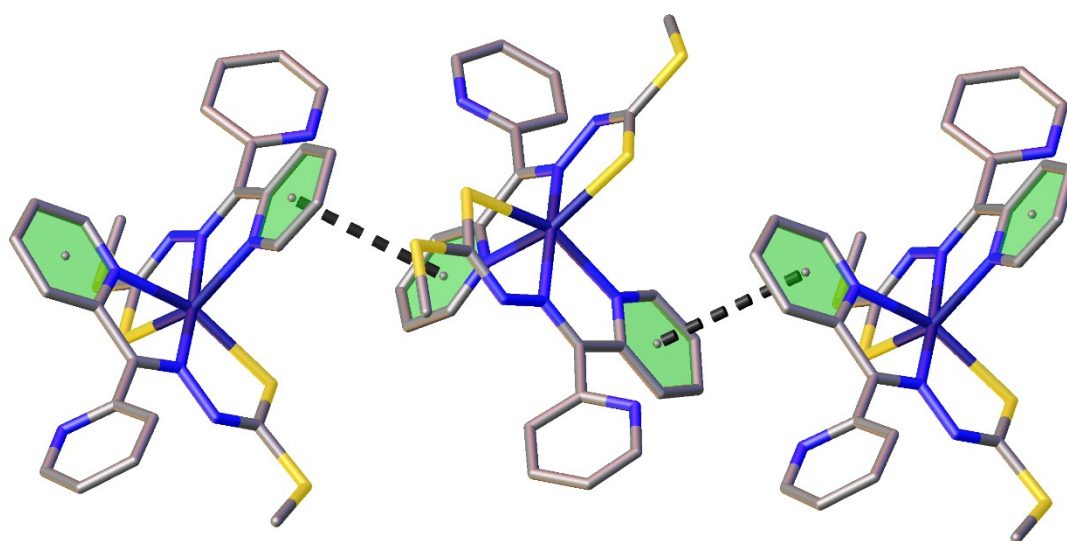


**Figure S2.** View of a 1D zigzag chain formed by  $\pi \cdots \pi$  stacking interactions (dashed lines) in complex Zn3. The H atoms are omitted for clarity.

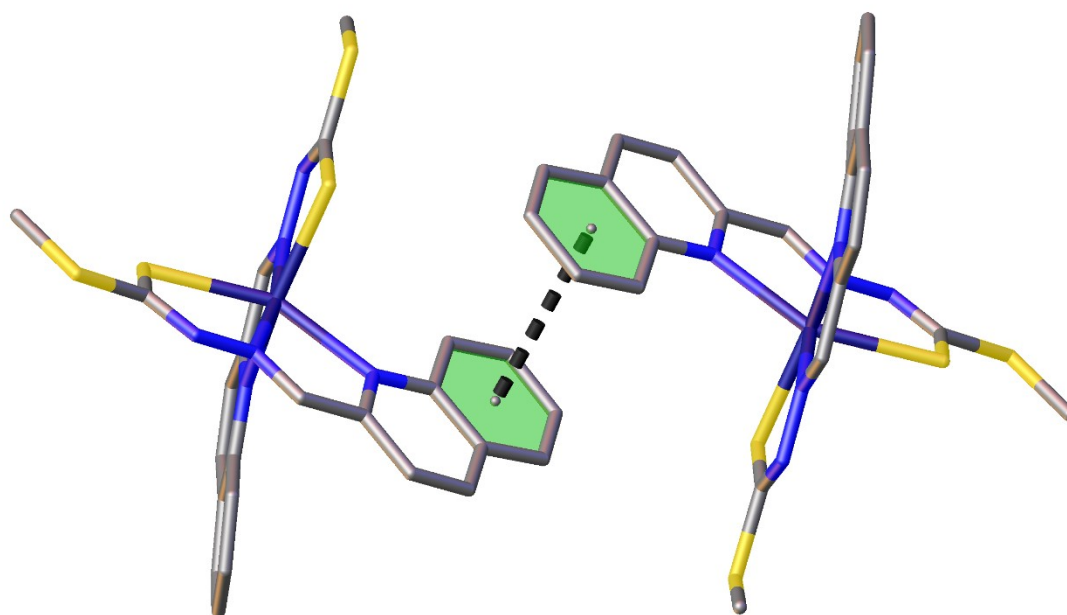


**Figure S3.** View of a dimeric structure formed by  $\pi \cdots \pi$  stacking interaction (dashed lines) in complex Zn4. The H atoms are omitted for clarity.

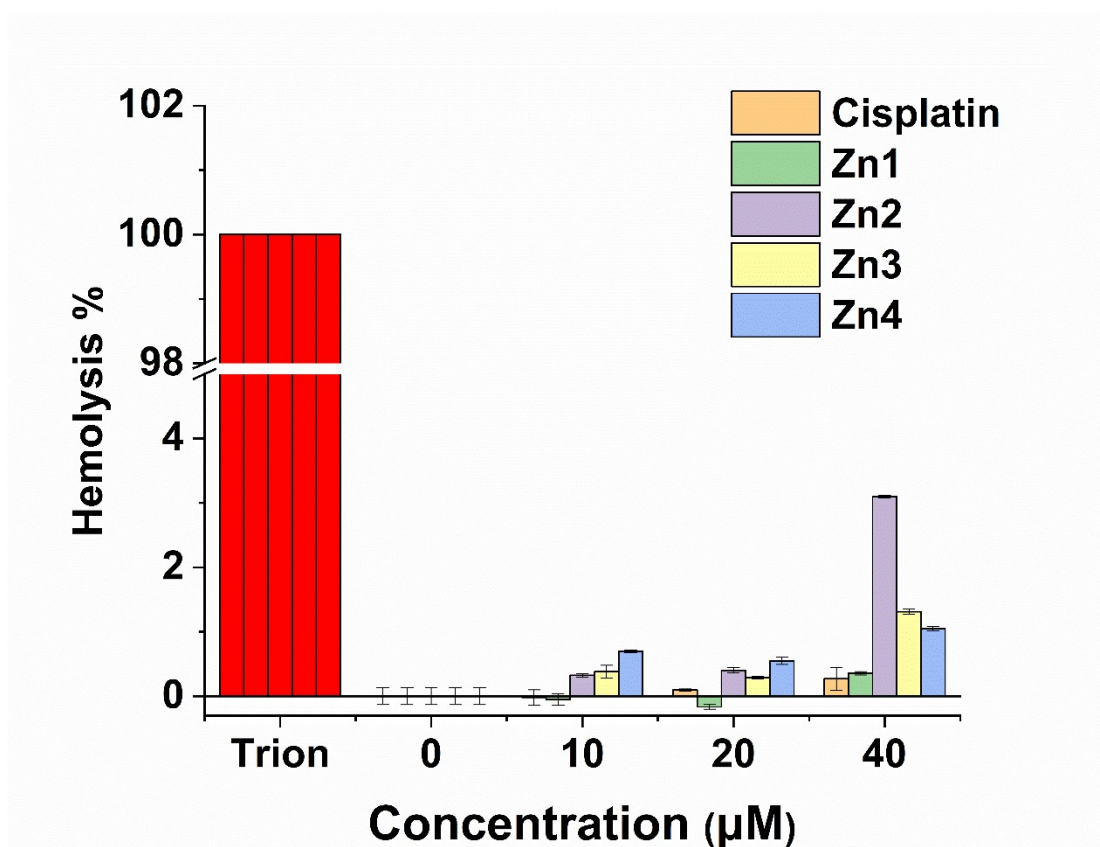
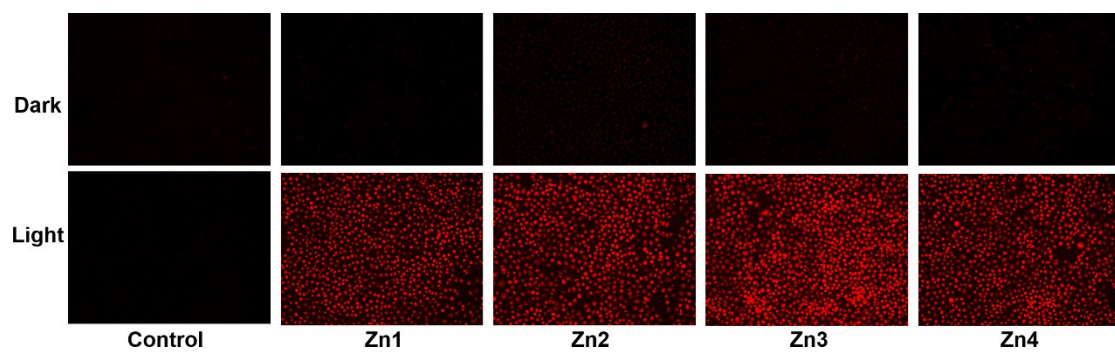
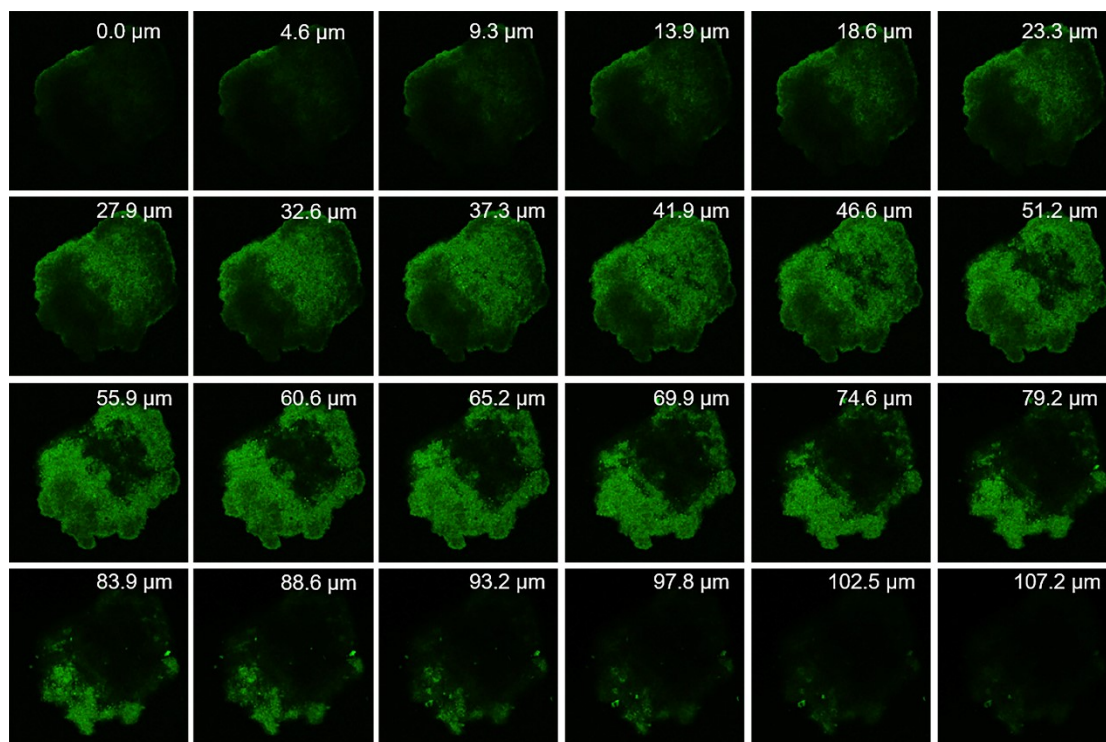


Figure S4. Human blood compatibility analysis of complexes Zn1-Zn4.



**Figure S5.** ROS determined by fluorescence microscopy in A549 cells.



**Figure S6.** Images of 3D A549 tumor spheres after incubation with complex Zn3 (10  $\mu\text{M}$ ) for 12 h. Excited Z-axis images scanning from the top to the bottom of an intact spheroid. The investigated complex Zn3 was detected under usage of its fluorescence properties ( $\lambda_{\text{ex}} = 488 \text{ nm}$ ,  $\lambda_{\text{em}} = 520\text{-}570 \text{ nm}$ ).

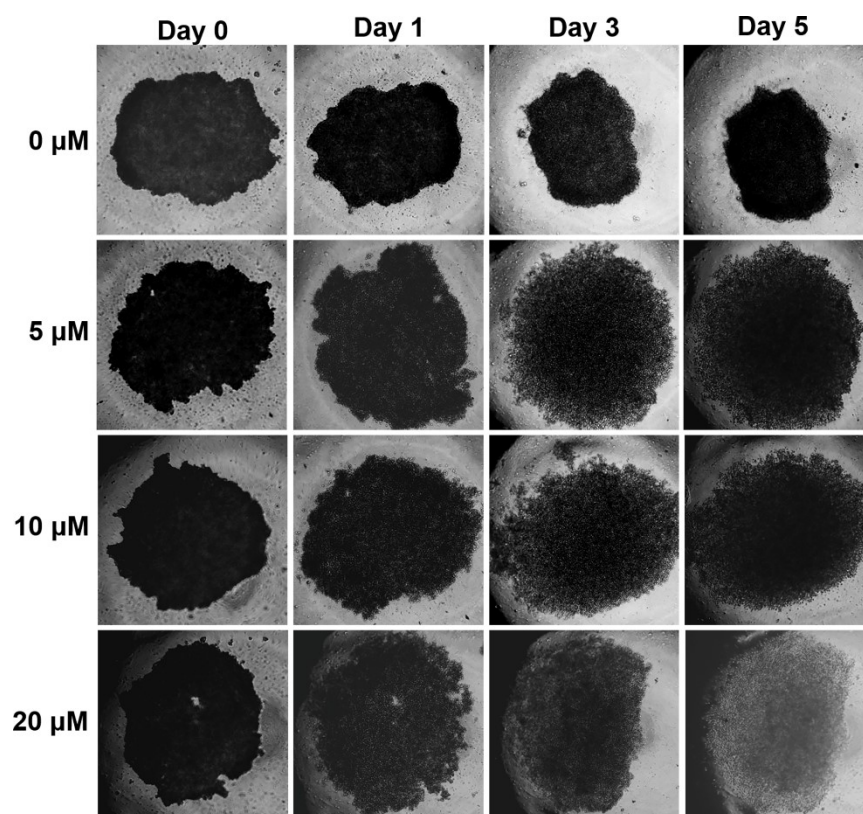


**Figure S7.** Morphology of 3D A549 tumor spheroids treated with complex Zn3 at the indicated concentrations for 5 days in the dark.

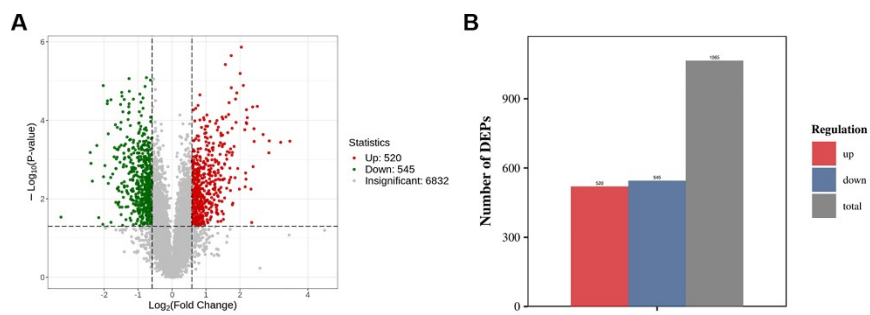


**Figure S8.** (A) Volcano plot of differentially expressed proteins. (B) Statistical histogram of differentially expressed proteins.

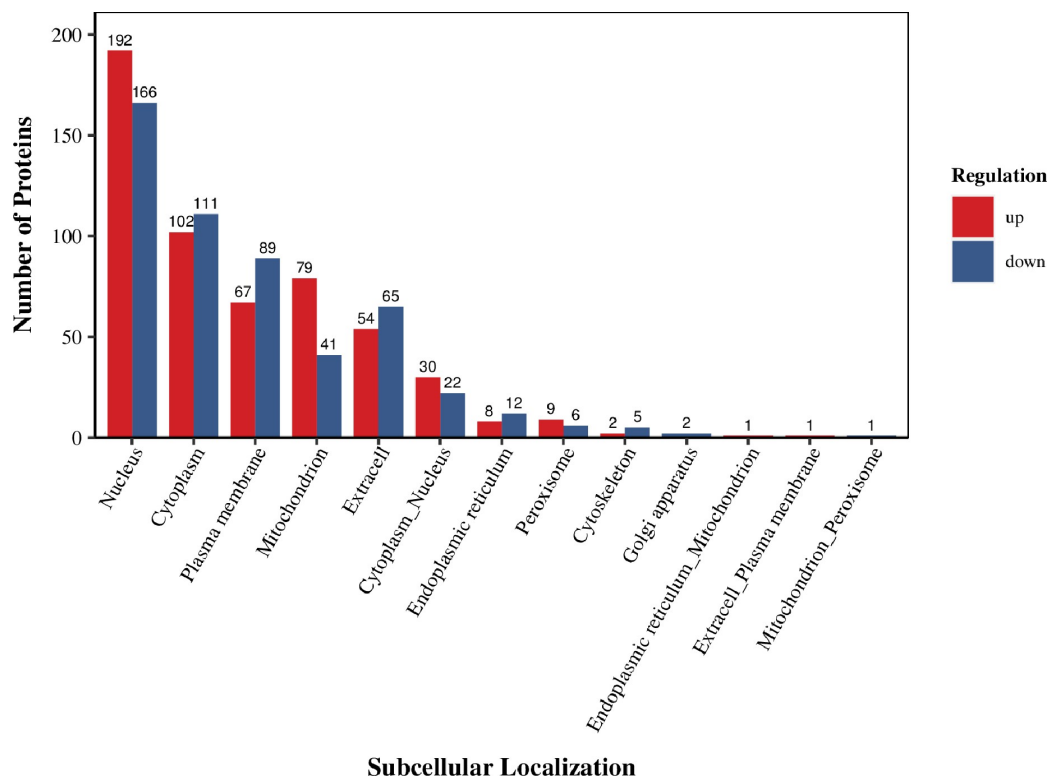


**Figure S9.** Subcellular localization of differentially expressed proteins.

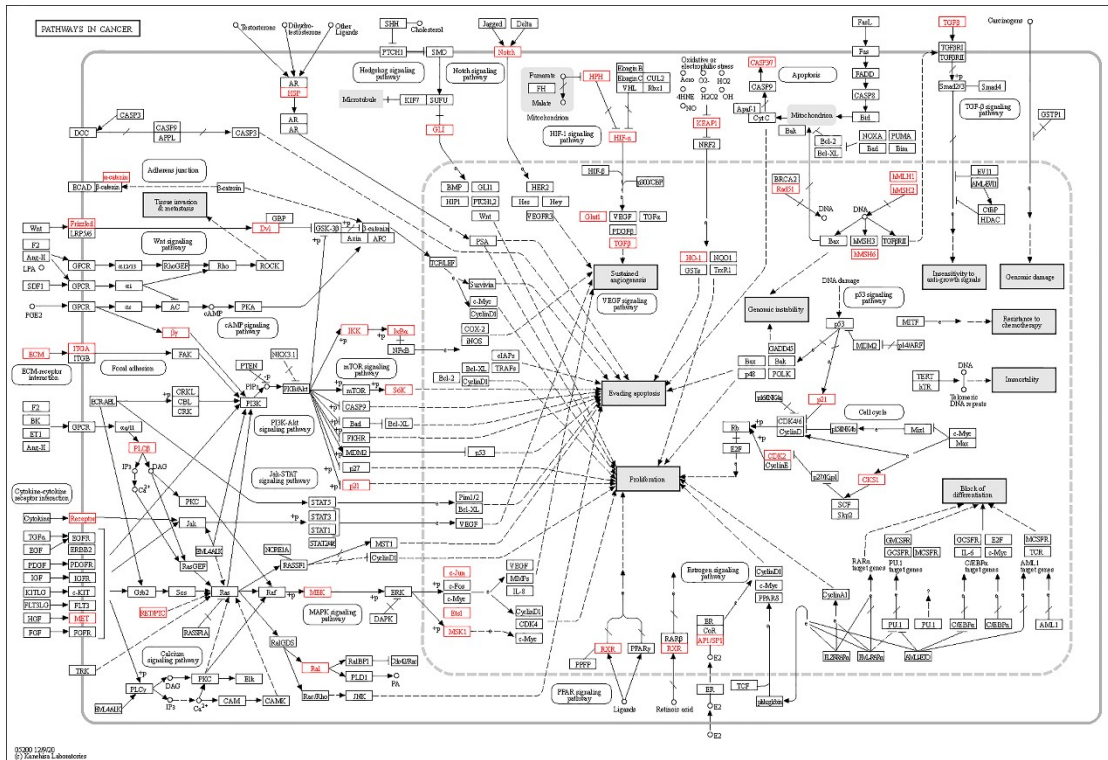


**Figure S10.** Network map of pathways in cancer pathway. Red: upregulated/downregulated DEPs. More details can be found on the website: <https://www.genome.jp/entry/map05200>.

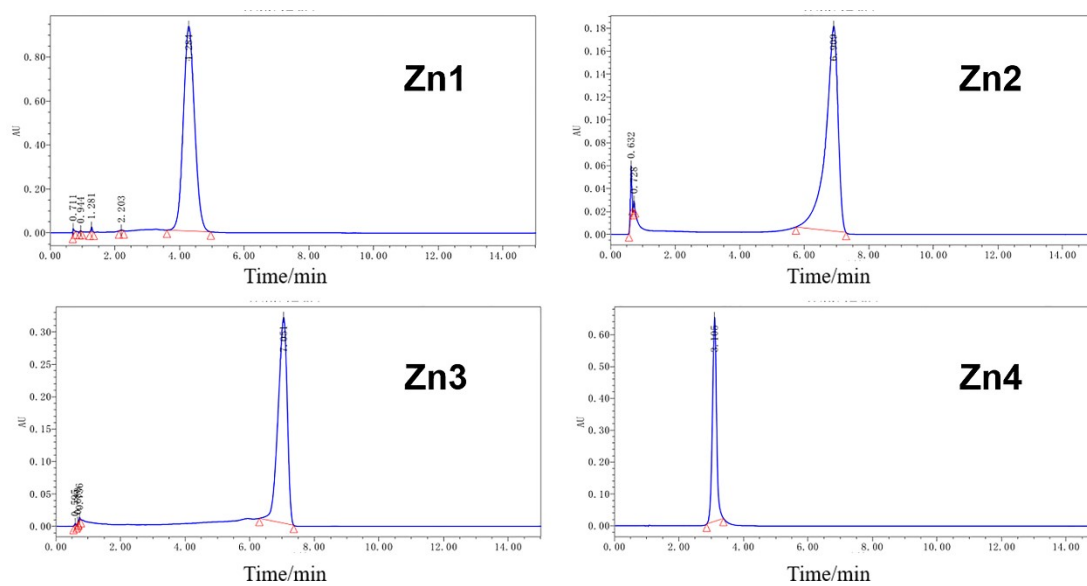


Figure S11. HPLC spectra for complexes Zn1-Zn4 (purity of complexes Zn1-Zn4 > 95%). Column: C18 column (SHIMADZU Shim-pack GIST-HP C18 2.1 $\phi$ 100 mm). Column temperature: 35 °C. Mobile phase: methanol/H<sub>2</sub>O (80:20) for Zn1 and acetonitrile/H<sub>2</sub>O (50:50) for Zn2-Zn3. Injection volume: 5  $\mu$ L. Flow rate: 0.3 ml/min.

**Table S1** Crystal data for Zn complexes **Zn1–Zn4**.

Complex	<b>Zn1</b>	<b>Zn2</b>	<b>Zn3</b>	<b>Zn4</b>
Empirical formula	C <sub>16</sub> H <sub>16</sub> N <sub>6</sub> S <sub>4</sub> Zn	C <sub>18</sub> H <sub>20</sub> N <sub>6</sub> S <sub>4</sub> Zn	C <sub>26</sub> H <sub>22</sub> N <sub>8</sub> S <sub>4</sub> Zn	C <sub>24</sub> H <sub>20</sub> N <sub>6</sub> S <sub>4</sub> Zn
Molecular weight	485.96	514.01	640.13	586.07
Crystal system	triclinic	monoclinic	monoclinic	monoclinic
Space group	<i>P</i> -1	<i>P</i> 2 <sub>1</sub> / <i>n</i>	<i>P</i> 2 <sub>1</sub> / <i>n</i>	<i>P</i> 2 <sub>1</sub> / <i>c</i>
<i>a</i> (Å)	8.6706(6)	13.8603(7)	10.9912(3)	14.5119(6)
<i>b</i> (Å)	10.5308(7)	11.4435(4)	16.5190(4)	17.9321(6)
<i>c</i> (Å)	12.9160(8)	15.5169(7)	15.7993(4)	10.3017(4)
$\alpha$ (°)	66.945(6)	90.00	90.00	90.00
$\beta$ (°)	81.930(5)	114.069(6)	95.001(3)	108.475(4)
$\gamma$ (°)	68.493(6)	90.00	90.00	90.00
<i>V</i> (Å <sup>3</sup> )	1009.57(11)	2247.16(18)	2857.65(13)	2542.64(17)
<i>Z</i>	2	4	4	4
$\rho_{\text{calc.}}$ (g·cm <sup>-3</sup> )	1.599	1.519	1.488	1.531
$\mu$ (Mo-K $\alpha$ ) (mm <sup>-1</sup> )	1.644	1.482	1.184	1.321
<i>F</i> (000)	496	1056	1312	1200
Data/restraint/parameters	4109/0/246	4592/0/266	5840/0/354	5191/1/312
Goodness-of-fit on <i>F</i> <sup>2 a</sup>	1.070	1.029	1.197	1.046
Final <i>R</i> <sub>1</sub> , <i>wR</i> <sub>2</sub> [ <i>I</i> > 2 $\sigma$ ( <i>I</i> )] <sup>b</sup>	0.0375, 0.0876	0.0375, 0.0851	0.0396, 0.0845	0.0388, 0.0902

<sup>a</sup> Goodness-of-fit =  $[\sum w(|F_o|^2 - |F_c|^2)|^2 / (N_{\text{observed}} - N_{\text{parameters}})]^{1/2}$ .

<sup>b</sup>  $R_1 = \sum ||F_o| - |F_c|| / \sum |F_o|$ .  $wR_2 = [\sum w(F_o^2 - F_c^2)^2 / \sum (F_o^2)^2]^{1/2}$ .  $w = 1 / [\sigma^2(F_o^2) + (aP)^2 + (bP)]$ .  $P = (\max(F_o^2 \text{ or } 0) + 2F_c^2) / 3$ .

**Table S2** Selected bond lengths [ $\text{\AA}$ ] and angles [ $^\circ$ ] in complexes **Zn1–Zn4**.

<b>Zn1</b>			
Zn1–S4	2.4532(8)	N2–Zn1–S4	111.16(6)
Zn1–S2	2.4567(7)	N2–Zn1–S2	79.14(6)
Zn1–N2	2.113(2)	N2–Zn1–N3	74.18(7)
Zn1–N3	2.2507(19)	N2–Zn1–N5	167.46(8)
Zn1–N5	2.114(2)	N2–Zn1–N6	94.50(8)
Zn1–N6	2.274(2)	N3–Zn1–S4	91.11(6)
S4–Zn1–S2	102.11(3)	N3–Zn1–S2	153.05(6)
N3–Zn1–N6	83.88(8)	N5–Zn1–S4	79.14(6)
N5–Zn1–S2	106.30(6)	N5–Zn1–N3	99.14(8)
N5–Zn1–N6	74.01(8)	N6–Zn1–S4	151.47(6)
<b>Zn2</b>			
Zn1–S4	2.4495(8)	N2–Zn1–S4	109.73(7)
Zn1–S2	2.4419(9)	N2–Zn1–S2	79.87(7)
Zn1–N2	2.128(2)	N2–Zn1–N3	73.78(9)
Zn1–N3	2.212(2)	N2–Zn1–N6	95.65(10)
Zn1–N5	2.114(2)	N3–Zn1–S4	91.10(6)
Zn1–N6	2.247(3)	N3–Zn1–S2	153.52(7)
S2–Zn1–S4	100.36(3)	N3–Zn1–N6	84.68(9)
N5–Zn1–S4	79.85(8)	N5–Zn1–S2	107.23(7)
N5–Zn1–N2	167.25(10)	N5–Zn1–N3	98.21(9)
N5–Zn1–N6	73.43(11)	N6–Zn1–S4	152.01(9)
<b>Zn3</b>			
Zn1–S2	2.4623(8)	N4–Zn1–S2	152.58(6)
Zn1–S4	2.4465(9)	N4–Zn1–S4	89.40(6)
Zn1–N4	2.228(2)	N2–Zn1–S2	78.94(6)
Zn1–N2	2.141(2)	N2–Zn1–S4	107.29(6)
Zn1–N8	2.217(2)	N2–Zn1–N4	73.64(8)
Zn1–N6	2.147(2)	N2–Zn1–N8	98.95(8)
S4–Zn1–S2	98.34(3)	N2–Zn1–N6	168.95(8)
N8–Zn1–S2	94.94(6)	N8–Zn1–S4	152.38(6)
N8–Zn1–N4	89.84(8)	N6–Zn1–S2	109.43(6)
N6–Zn1–S4	79.17(6)	N6–Zn1–N4	97.84(8)
<b>Zn4</b>			
Zn1–S2	2.4575(8)	N6–Zn1–S2	98.29(6)

Zn1-S4	2.5178(9)	N6-Zn1-S4	149.69(6)
Zn1-N6	2.263(2)	N6-Zn1-N3	86.08(8)
Zn1-N3	2.376(2)	N3-Zn1-S2	151.23(5)
Zn1-N5	2.114(2)	N3-Zn1-S4	92.84(6)
Zn1-N2	2.120(2)	N5-Zn1-S2	99.69(7)
S2-Zn1-S4	97.06(3)	N5-Zn1-S4	77.16(7)
N5-Zn1-N6	74.59(8)	N5-Zn1-N3	108.85(8)
N5-Zn1-N2	172.07(8)	N2-Zn1-S2	79.33(6)
N2-Zn1-S4	95.10(6)	N2-Zn1-N6	113.34(8)

---

**Table S3** Interaction energy decomposition (kcal/mol) of the dimers formed by  $\pi \cdots \pi$  stacking interaction in these complexes obtained from the EDA-FF analysis.<sup>a</sup>

Complexes	$E^{\text{int}}$	$E^{\text{ele}}$	$E^{\text{rep}}$	$E^{\text{disp}}$
dimer in Zn1	-52.53	-15.78	27.00	-63.74
dimer in Zn3	-61.05	-17.37	25.05	-68.73
dimer in Zn4	-51.99	-10.89	23.37	-64.47

<sup>a</sup> The total intermolecular interaction energy ( $E^{\text{int}}$ ) can be decomposed into repulsion ( $E^{\text{rep}}$ ), electrostatic ( $E^{\text{ele}}$ ), and dispersion ( $E^{\text{disp}}$ ) energies:  $E^{\text{int}} = E^{\text{rep}} + E^{\text{ele}} + E^{\text{disp}}$ .

**Table S4.** The charge transfer properties between Zn and ligands in the UV-vis absorption spectra of complexes **Zn1–Zn4**.

complex	state	f	$\lambda_{cal}$ (nm)	Ligand-to-ligand (Contribution %)	Zn-to-ligand (Contribution %) <sup>a</sup>
Zn1	1	0.107	421.6	95.8	
	2	0.0824	412	96.7	
	3	0.2702	390.2	93.9	
	4	0.2549	387.3	95.9	
	5	0.0356	380.1	90.2	8.1
	6	0.1585	376.9	92.6	5.7
	7	0.0041	359.8	89.6	8.6
	8	0.1738	353.3	90.9	7.3
	9	0.1504	329.4	97.3	
	10	0.1249	326.3	97.4	
	11	0.0217	321.1	95.6	
	12	0.1202	320.8	95.7	
	13	0.0569	294.2	95.9	
	14	0.0023	293.4	91.6	6.8
	15	0.0064	291.9	93	5.4
	16	0.0569	289.1	97.5	
	17	0.0292	282.1	97.4	
	18	0.0218	278.1	98	
	19	0.0043	274.7	91.1	7.2
	20	0.0005	274.4	90.9	7.4
Zn2	1	0.0777	413.2	95.6	
	2	0.0629	402.8	96.3	
	3	0.1071	379.3	91.9	6.5
	4	0.1137	376.9	92.4	6

---

5	0.024	369.2	92.3	6.1
6	0.1695	364.1	94.1	
7	0.0005	358.7	90	8.4
8	0.1406	350.1	91.8	6.6
9	0.2574	332.6	97.9	
10	0.2514	328.9	97.5	
11	0.001	327.1	97.2	
12	0.1228	325.5	97.1	
13	0.0476	296.5	96	
14	0	294.8	92.7	5.9
15	0.0055	293.8	92.8	5.7
16	0.0312	291.9	96.4	
17	0.0259	280	96.6	
18	0.0229	277	96.8	
19	0.0098	274.8	90.4	8.1
20	0.0042	274.7	90.5	8

---

Zn3	1	0.1204	442.2	95.5	
	2	0.0598	421.5	96.4	
	3	0.1189	405.2	92.7	5.6
	4	0.0743	401.1	92.2	6.3
	5	0.0458	387.8	92.8	5.5
	6	0.1627	384	94	
	7	0.01	377.1	90.1	8.4
	8	0.1106	368.3	92.6	5.8
	9	0.1917	354.4	97.8	
	10	0.1789	350.5	96.9	
	11	0.0497	344.7	97.7	
	12	0.0475	342.4	96.9	

---

	13	0.0219	312.1	92.7	5.6
	14	0.0218	310.7	92.4	6
	15	0.0737	292.4	96.7	
	16	0.0247	292	97.5	
	17	0.0007	291	95	
	18	0.0005	290.3	97.3	
	19	0.0132	285.6	95.5	
	20	0.0054	284.2	95.3	
Zn4	1	0.0753	469.4	96.8	
	2	0.1019	453.9	96.9	
	3	0.1838	427.9	95.6	
	4	0.3142	426.5	95.5	
	5	0.021	412.1	90.2	8.1
	6	0.0153	408.2	90.6	7.7
	7	0.0591	396	90.5	7.9
	8	0.1765	387.3	91.3	7.1
	9	0.1378	370.4	97.6	
	10	0.1839	365.6	97.6	
	11	0.0127	359.5	96.5	
	12	0.131	347.9	96.5	
	13	0.0294	339.7	98	
	14	0.0351	338.5	98	
	15	0.001	329.1	98.1	
	16	0.0008	323.9	98	
	17	0.0037	318.4	92.2	6.1
	18	0.006	316.9	92	6.3
	19	0.0737	306.8	98.2	
	20	0.1165	305.4	98.2	

<sup>a</sup>: Contribution (%) larger than 5% are shown.

**Table S5.** Details for the differentially expressed proteins involved in some significant KEGG pathways.

KEGG Pathways	DiffSeqs	Gene Name	Up/Down (Ratio)	DiffSeqs	Gene Name	Up/Down (Ratio)
Pathways in cancer	O14640	DVL1	0.622773795	O15111	CHUK	0.600223257
	O15230	LAMA5	0.429711981	O75582	RPS6KA5	0.615117304
	P01137	TGFB1	0.6461974	P02462	COL4A1	3.42321063
	P05412	JUN	2.833259802	P07942	LAMB1	0.438963643
	P08572	COL4A2	2.363095685	P08581	MET	0.549627707
	P09601	HMOX1	5.704677693	P10070	GLI2	0.509030105
	P11047	LAMC1	0.511167254	P11166	SLC2A1	2.312111773
	P11234	RALB	1.615258559	P14921	ETS1	2.50204509
	P17301	ITGA2	2.259212033	P19793	RXRA	0.636137732
	P24941	CDK2	1.587634415	P25963	NFKBIA	0.604854098
	P38936	CDKN1A	4.569418428	P40692	MLH1	0.646430702
	P43246	MSH2	0.619512999	P46531	NOTCH1	2.619701554
	P50151	GNG10	0.508440224	P52701	MSH6	0.571362399
	P55210	CASP7	0.530613745	P61024	CKS1B	1.711624975
	P78552	IL13RA1	0.638129396	Q02750	MAP2K1	1.624750543
	Q04721	NOTCH2	2.000431005	Q06609	RAD51	1.916255012

	Q13751	LAMB3	2.347022246	Q13772	NCOA4	3.019669345
	Q14145	KEAP1	0.53775123	Q14332	FZD2	0.412750979
	Q15147	PLCB4	0.616236738	Q16665	HIF1A	3.622003303
	Q16787	LAMA3	0.454015142	Q58FG1	HSP90AA4 P	2.791812525
	Q9GZT9	EGLN1	2.574063373	Q9UBS0	RPS6KB2	0.559456643
	Q9UBT7	CTNNAL1	0.578285608			
p53 signaling pathway	O00220	TNFRSF10A	1.778690297	O14763	TNFRSF10 B	3.237735365
	O15297	PPM1D	2.066377021	P24941	CDK2	1.587634415
	P31350	RRM2	1.913879066	P38936	CDKN1A	4.569418428
	P49815	TSC2	0.511000911	P58004	SESN2	9.18957579
	Q13315	ATM	0.619152557	Q13535	ATR	0.530721645
	Q7LG56	RRM2B	1.524901652			
HIF-1 signaling pathway	F5GZQ4	LDHA	2.390454365	P00558	PGK1	1.603459297
	P01033	TIMP1	3.352808216	P07205	PGK2	1.553907043
	P09104	ENO2	1.78641635	P09601	HMOX1	5.704677693
	P09972	ALDOC	3.752273923	P11166	SLC2A1	2.312111773
	P36941	LTBR	0.548366052	P38936	CDKN1A	4.569418428
	P52789	HK2	1.662738447	Q02750	MAP2K1	1.624750543

	Q16665	HIF1A	3.622003303	Q16875	PFKFB3	5.325252427
	Q9GZT9	EGLN1	2.574063373	Q9UBS0	RPS6KB2	0.559456643
PI3K-Akt signaling pathway	O14944	EREG	0.103714479	O15111	CHUK	0.600223257
	O15230	LAMA5	0.429711981	O43524	FOXO3	1.921283913
	P02462	COL4A1	3.42321063	P07942	LAMB1	0.438963643
	P08572	COL4A2	2.363095685	P08581	MET	0.549627707
	P08648	ITGA5	1.6553973	P11047	LAMC1	0.511167254
	P13807	GYS1	2.493982955	P17301	ITGA2	2.259212033
	P19793	RXRA	0.636137732	P24941	CDK2	1.587634415
	P35568	IRS1	0.650406236	P38936	CDKN1A	4.569418428
	P49815	TSC2	0.511000911	P50151	GNG10	0.508440224
	P54646	PRKAA2	1.887107324	Q02750	MAP2K1	1.624750543
	Q07820	MCL1	2.565034598	Q13751	LAMB3	2.347022246
	Q16787	LAMA3	0.454015142	Q16822	PCK2	1.896549758
	Q58FG1	HSP90AA4P	2.791812525	Q99650	OSMR	1.800425318
	Q9NX09	DDIT4	2.596634697	Q9UBS0	RPS6KB2	0.559456643
ECM-receptor interaction	O00468	AGRN	0.454888657	O15230	LAMA5	0.429711981
	P02462	COL4A1	3.42321063	P07942	LAMB1	0.438963643
	P08572	COL4A2	2.363095685	P08648	ITGA5	1.6553973
	P11047	LAMC1	0.511167254	P17301	ITGA2	2.259212033

	P18827	SDC1	0.391008078	P98160	HSPG2	0.332549285
	Q13751	LAMB3	2.347022246	Q14118	DAG1	0.318826123
	Q16787	LAMA3	0.454015142			
Cytokine- cytokine receptor interaction	O00220	TNFRSF10A	1.778690297	O14763	TNFRSF10 B	3.237735365
	P01137	TGFB1	0.6461974	P18075	BMP7	0.583236467
	P36941	LTBR	0.548366052	P41273	TNFSF9	3.319471852
	P78552	IL13RA1	0.638129396	Q8IUW5	RELL1	1.53367019
	Q99650	OSMR	1.800425318	Q9NP84	TNFRSF12 A	3.549476687
	Q9NPH3	IL1RAP	4.590931959			

## Notes and references

1. S. Cheng-Yong, Y. Xiao-Ping, K. Bei-Sheng, Y. Kai-Bei, T. Ye-Xiang and M. T. Cong-Wai, Syntheses and Crystal Structures of Methyl 2-Pyridylmethylidenehydrazinecarbodithioate and of Its Copper(II) Complex: Supramolecular Arrays Exhibiting pseudo-Helical Arrangement Controlled by Hydrogen Bonding or S $\cdots$ S Contact, *Bull. Chem. Soc. Jpn.*, 1999, **72**, 2217-2222.
2. M. Akbar Ali, A. H. Mirza, M. H. S. A. Hamid and P. V. Bernhardt, Diphenyltin(IV) complexes of the 2-quinolinecarboxaldehyde Schiff bases of S-methyl- and S-benzylidithiocarbamate (Hqaldsme and Hqaldsbz): X-ray crystal structures of Hqaldsme and two conformers of its diphenyltin(IV) complex, *Polyhedron*, 2005, **24**, 383-390.
3. M. T. Basha, J. D. Chartres, N. Pantarat, M. Akbar Ali, A. H. Mirza, D. S. Kalinowski, D. R. Richardson and P. V. Bernhardt, Heterocyclic dithiocarbamate iron chelators: Fe coordination chemistry and biological activity, *Dalton Trans.*, 2012, **41**, 6536-6548.
4. O. V. Dolomanov, L. J. Bourhis, R. J. Gildea, J. A. K. Howard and H. Puschmann, OLEX2: a complete structure solution, refinement and analysis program, *J. Appl. Crystallogr.*, 2009, **42**, 339-341.
5. M. J. Frisch, G. W. Trucks, H. B. Schlegel, G. E. Scuseria, M. A. Robb, J. R. Cheeseman, G. Scalmani, V. Barone, G. A. Petersson, H. Nakatsuji, X. Li, M. Caricato, A. V. Marenich, J. Bloino, B. G. Janesko, R. Gomperts, B. Mennucci, H. P. Hratchian, J. V. Ortiz, A. F. Izmaylov, J. L. Sonnenberg, D. Williams-Young, F. Ding, F. Lipparini, F. Egidi, J. Goings, B. Peng, A. Petrone, T. Henderson, D. Ranasinghe, V. G. Zakrzewski, J. Gao, N. Rega, G. Zheng, W. Liang, M. Hada, M. Ehara, K. Toyota, R. Fukuda, J. Hasegawa, M. Ishida, T. Nakajima, Y. Honda, O. Kitao, H. Nakai, T. Vreven, K. Throssell, J. A. Montgomery, Jr., J. E. Peralta, F. Ogliaro, M. J. Bearpark, J. J. Heyd, E. N. Brothers, K. N. Kudin, V. N. Staroverov, T. A. Keith, R. Kobayashi, J. Normand, K. Raghavachari, A. P. Rendell, J. C. Burant, S. S. Iyengar, J. Tomasi, M. Cossi, J. M. Millam, M. Klene, C. Adamo, R. Cammi, J. W. Ochterski, R. L. Martin, K. Morokuma, O. Farkas, J. B. Foresman, D. J. Fox, Gaussian 16 Rev. A.03, Gaussian, Inc., Wallingford CT, 2016.

6. T. Lu and F. Chen, Multiwfn: A multifunctional wavefunction analyzer, *J. Comput. Chem.*, 2012, **33**, 580-592.
7. Z. Liu, X. Wang, T. Lu, A. Yuan and X. Yan, Potential optical molecular switch: Lithium@cyclo[18]carbon complex transforming between two stable configurations, *Carbon*, 2022, **187**, 78-85.
8. T. Lu, Z. Liu and Q. Chen, Comment on "18 and 12 – Member carbon rings (cyclo[n]carbons) – A density functional study", *Mat. Sci. Eng. B-Adv*, 2021, **273**, 115425.
9. M. K. M. Subarkhan and R. Ramesh, Ruthenium(ii) arene complexes containing benzhydrazone ligands: synthesis, structure and antiproliferative activity, *Inorg. Chem. Front.*, 2016, **3**, 1245-1255.
10. R. Bevernaegie, B. Doix, E. Bastien, A. Diman, A. Decottignies, O. Feron and B. Elias, Exploring the Phototoxicity of Hypoxic Active Iridium(III)-Based Sensitizers in 3D Tumor Spheroids, *J. Am. Chem. Soc.*, 2019, **141**, 18486-18491.
11. V. Novohradsky, A. Rovira, C. Hally, A. Galindo, G. Viguera, A. Gandioso, M. Svitelova, R. Bresolí-Obach, H. Kostrhunova, L. Markova, J. Kasparkova, S. Nonell, J. Ruiz, V. Brabec and V. Marchán, Towards Novel Photodynamic Anticancer Agents Generating Superoxide Anion Radicals: A Cyclometalated Ir(III) Complex Conjugated to a Far-Red Emitting Coumarin, *Angew. Chem. Int. Ed. Engl.*, 2019, **58**, 6311-6315.
12. Y. Gou, X. Jia, L. X. Hou, J. G. Deng, G. J. Huang, H. W. Jiang and F. Yang, Dithiocarbamate-Fe(III), -Co(III), -Ni(II), and -Zn(II) Complexes: Design, Synthesis, Structure, and Anticancer Evaluation, *J. Med. Chem.*, 2022, **65**, 6677-6689.